Integrated optics on Lithium Niobate for sensing applications

A. Zaltron, G. Bettella, G. Pozza, R. Zamboni, M. Ciampolillo, N. Argiolas, C. Sada*
Physics and Astronomy Department "Galileo Galilei", University of Padova, Via Marzolo 8, 35131 Padova (Italy)

S. Kroesen, M. Esseling, C. Denz
Nonlinear Photonics Group, Institute of Applied Physics, University of Münster Corrensstrasse 2/4, 48149 Münster (Germany)

*Corresponding author
email: cinzia.sada@unipd.it

ABSTRACT

In micro-analytical chemistry and biology applications, optofluidic technology holds great promise for creating efficient lab-on-chip systems where higher levels of integration of different stages on the same platform is constantly addressed. Therefore, in this work the possibility of integrating opto-microfluidic functionalities in lithium niobate ($LiNbO_3$) crystals is presented. In particular, a T-junction droplet generator is directly engraved in a $LiNbO_3$ substrate by means of laser ablation process and optical waveguides are realized in the same material by exploiting the Titanium in-diffusion approach. The coupling of these two stages as well as the realization of holographic gratings in the same substrate will allow creating new compact optical sensor prototypes, where the optical properties of the droplets constituents can be monitored.

Keywords: optofluidics, lithium niobate, T-junctions, optical waveguides, integrated optics

1. INTRODUCTION

In the last years, many efforts were directed by the scientific community toward developing of new microfluidic devices, which have significantly advanced from their root in micro-analytical chemistry to include high throughput screening, biological analysis of cells and proteins, reaction kinetics and mechanism studies[1]. In particular the droplet microfluidics has received great attention thanks to its scalability and parallel processing, which allow realizing a wide range of applications, from the synthesis of biomolecules to drug delivery and bio-sensing [2, 3]. Although novel micro-fabrication techniques are continuously being developed and micro-chemical systems are established by integrating micro-devices with appropriate fluidic interfacing scheme, the incorporation of chemical and physical optical sensors perfectly integrated with the micro-reactor stage is still under debate. In this scenario, the integration of a large number of different stages on a single substrate chip is a key point for promoting new insights in many applications that need portable devices to speed the analysis and investigate new phenomena [4, 5]. Among the others, even lithium niobate ($LiNbO_3$) crystals have been proposed in microfluidics, since it allows for high efficient acoustic waves generation to move droplets on the substrate in a very controlled way [6], as well as flow mixing and pumping[7], pyroelectric[8] and photogalvanic[9-12] particle trapping and so on. Quite surprisingly, all the above mentioned applications were realized without producing a microfluidic circuit directly on the $LiNbO_3$ substrates and without the integration of optical sensing stages, although this material is thoroughly exploited in the photonic and integrated optics industry. As a matter of fact, besides the realization of several electro-optical devices, lithium niobate is used for realizing various optical systems, such as second-harmonic generation, optical modulators, waveguides and so on, thanks to its remarkable optical coefficients and significant photorefractive response.
That being so, recently also lithium niobate has been proposed as candidate for application in opto-microfluidic technology[13], thus combining the tools typical of microfluidics with the potentialities offered by this material. As

Optical Sensors 2015, edited by Francesco Baldini, Jiri Homola, Robert A. Lieberman, Proc. of SPIE
Vol. 9506, 950608 · © 2015 SPIE · CCC code: 0277-786X/15/$18 · doi: 10.1117/12.2178457

a matter of fact, the integration on the same $LiNbO_3$ substrate of different functionalities would allow obtaining new systems able to perform on-site optical sensing processes, such as those required in chemical and biological analyses. The realization of such a device prototypes requires different preparation steps, from the creation of the microfluidic droplet generation to the implementation of channel waveguides for the optical sensing of the droplets. In this way, besides the droplet formation, the circuit would be able to transfer the liquids through a microfluidic channel directly engraved on the crystal substrate up to an integrated analysis stage where the optical properties of the droplet constituents are monitored and detected.
In this work, we will describe the recent results on the realisation and characterization of each of the mentioned stages on lithium niobate crystals, with the aim of addressing the potential realization of optical sensing platforms. In particular, the droplet generator was realized on $LiNbO_3$ substrates by engraving T-junctions using the laser ablation technique[14], while the optical waveguide coupled to the microfluidic channels were integrated on the same substrate by exploiting Ti in-diffusion process on photolithographically patterned waveguides.

2. EXPERIMENTAL

2.1 Microfluidic stage

A pure x-cut $LiNbO_3$ sample with congruent composition was cut from a commercial wafer (Crystal Tech.) polished on both sides. The T-junction was realized on the lithium niobate substrate by using a Ti:Sapphire femtosecond laser (Coherent Inc.), with an operating wavelength of 800 nm, 1 kHz repetition rate and 120 fs pulse length. The laser beam was focused at the surface of the crystal by using a 50x ultralong working distance microscope objective (NA=0.55) equipped with a computer-controlled XYZ translation stage, which allows moving the $LiNbO_3$ sample with high spatial resolution. The experimental parameters used for the realization of the microfluidic circuits have been previously optimized [14], so that in this work the scanning speed and the energy pulse were set to 500 μm/s and 5 μJ, respectively. The sizes of the engraved microfluidic channels were measured by using a surface profilometer (KLA Tencor P-10): the depth was estimated close to h = (100 ±1) μm while their width was w = (125 ±3) μm, with a roughness at the micro-channel bottom of the order of R_a = (0.26 ± 0.02) μm. Finally, the T-junction was sealed with a thick layer of polydimethylsiloxane (PDMS) where the inlet and outlet reservoirs have been previously realized accordingly to the sizes of the microfluidic circuit. The PDMS structure was bounded to the lithium niobate substrate by using a O_2-plasma treatment (plasma system FEMTO) for 60 s at 200 W, with an oxygen flow rate of 10 sccm at $3x10^{-3}$ mbar.
Droplets were realized inside the $LiNbO_3$-based T-junction circuit by mixing two immiscible liquids through flexible polyethylene tubes (0.5 mm ID). Hexadecane ($CH_3(CH_2)_{14}CH_3$, CAS number: 544-76-3, viscosity 3cP, density 0.77 g/cm^3) and distilled water were used as continuous phase and dispersed phase, respectively [15], and they were injected into the microfluidic channels by using two independent automated syringe pumps (PHD 2000, Harvard Apparatus), working at constant flow rates between 1 and 500 mL/min. Moreover, $LiNbO_3$ was completely wetted by the hexadecane, but demonstrated to be moderately hydrophobic, presenting with these two liquids a contact angle minor of 10° and close to 60°, respectively. The images of the droplet generated by the T-junctions were recorded using a monochrome camera (MV D1024 CMOS, Photonfocus) coupled to an inverted microscope (Eclipse Ti-E, Nikon), whereas the videos were acquired by using the fast camera Phantom VRI v7.3.

2.2 Optical stage

Besides the realization of the T-junction droplet generator, the second important step to create an opto-fluidic device is the creation of the optical waveguides which will be coupled to the microfluidic channels, in order to get the final device prototype sketched in Fig.1. The waveguides were realized by exploiting the standard Titanium in-diffusion process: Ti strips are deposited on the lithium niobate substrates by using the RF sputtering technique combined with masked open channels realised by standard photolithographic method [16]; then the Ti strips are diffused inside the lithium niobate substrate by means of high temperature thermal treatments, thus obtaining in-diffused channel waveguides. Concerning the deposition of Titanium, the sputtering process was carried out at power and pressure of 80W and $5x10^{-3}$ mbar, respectively, while the sample was maintained under rotation to homogenize the Ti deposition. The Rutherford Back-Scattering technique was used to estimate the Ti deposition rate, which was found to be close to (47 ± 2) x 10^{15} at/(cm^2 s). The Ti strips (width equals to (9.8 ± 0.5) μm or (5.9 ± 0.2) μm) were in-

diffused by performing thermal treatments in a tubular furnace at 1030°C for 2h in air or O_2 atmosphere. The resulting Titanium in-depth profile was determined by means of Secondary Ion Mass Spectrometry (SIMS) measurements. A magnetic sector SIMS instrument by CAMECA (model ims-4f) was used, by exploiting the Cs^+ primary beam, with an impact energy of 14.5 keV.
The Near Field method was used to study the light intensity distribution of the beam exiting the optical waveguides, thus testing their performances. In these measurements the single mode beam exiting a fiber-coupled diode laser at 670 nm was injected into the Ti:LN waveguides by exploiting a spherical lens (f = 20mm) and a microscope objective (magnification 20x, NA = 0.4). At the output of the optical waveguide the near-field image was collected by a Vidicon tube equipped with a microscope objective (20x, f = 10 mm) in order to enlarge the beam spot before entering the digital camera system (LaserCam-HR, Coeherent), which allows to study as the intensity distribution of the guided beam varies accordingly to the geometrical sizes of the channel waveguides.

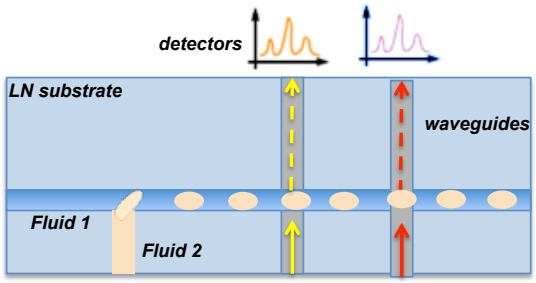

Fig.1 Sketch of the opto-fluidics device prototype.

3. RESULTS

The relative performances of each stage of the opto-microfluidic prototype were characterized and optimize, in order to get the best coupling efficiency between the microfluidic channel and the guided light beam.

3.1 Microfluidic stage: T-junction characterization

Droplets were formed inside the $LiNbO_3$-based T-junction by varying the fluxes Q_C and Q_D of the continuous (C, hexadecane) and dispersed (D, distilled water) phases, respectively. The values of the flux Q_C and the viscosity μ_C (3.0041 mPa·s at 25°C) of the continuous phase determine the value of capillary number C_a of the microfluidic system, the capillary number being defined as

$$Ca = \mu_C \cdot Q_C/(\sigma \cdot w \cdot h) \quad (1)$$

where σ is the interface energy between the two liquids. In particular in our experiments the value of Q_C was varied between 5 μL/min and 40 μL/min, leading to values of C_a in the range 0.0004÷0.0032. Concerning the interface energy σ at the water-oil interface, its value can be easily decreased by adding the proper surfactant to the hexadecane, thus also facilitating droplets formation. In our case the SPAN® 80 surfactant was used with a concentration set to 0.08% (w/w), which is above the critical micelle concentration (0.03% (w/w) for hexadecane [15]. In this case, a reduction of a factor 5 in the surface tension σ was obtained since in pure hexadecane $\sigma_0 = (50.7 \pm 0.3)$ mN/m, whereas it is reduced to $\sigma_{surfactant} = (10 \pm 0.3)$ mN/m when adding the SPAN®80. Finally, the droplet generation frequency was tested from 3.65 Hz up to 315.7 Hz when the surfactant was added to the continuous phase, while the investigated frequency range was between 1.77 Hz and 364.3 Hz in absence of SPAN® 80.
In the following discussion the model proposed by Christopher et al. [17] was taken as reference to characterize and evaluate the performance of our T-junction droplet generator. In Christopher's theory, the process of droplet formation is analysed in the frame of the competition between the local fluid shear stress, that acts to deform the

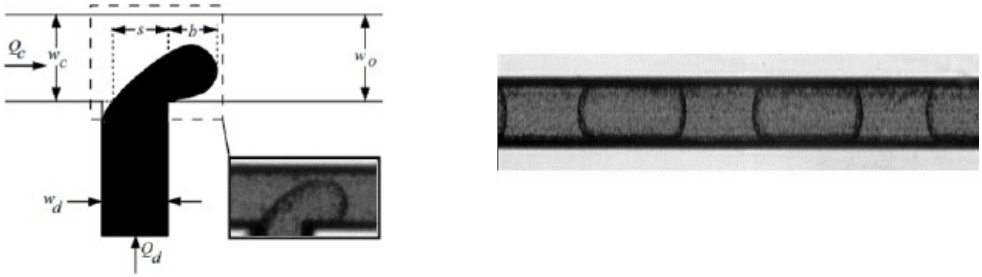

(a) (b)

Fig.2 (a) typical dynamics of the droplet formation in a T-junction circuit and main parameters which rule the squeezing regime; (b) droplets moving in the microfluidic channel investigated in this work (Q_C=12 mL/min, Q_D=40 mL/min.

interface, and the capillary pressure ΔP_L, which resists to that deformation, thus taking into account both the squeezing and the dripping regimes. However, in this work the attention was focused on the squeezing regime of the droplet formation process, which is when the dispersed phase obstructs the channel as the droplet grows, thus restricting the flow of the continuous phase. This restriction produces an increase of the dynamic pressure upstream of the droplets that generates a force necking the interface and pinching off the droplets [18]. This configuration generally occurs at low velocity of both liquid phases and for a channel width ratio $\Lambda = w_C/w_D$ close to 1, as it is the case of our microfluidic circuit. In particular, Christopher's model predicts that in this regime the length L of the droplet depends not only on Λ, but also on the ratio of the flow rates $\phi = Q_D/ Q_C$ as well as on a geometrical factor b (depicted in Fig.2). Therefore, the following relation holds

$$L_{eff} = \bar{b} + \frac{\Lambda}{\bar{b}} \cdot \phi \tag{2}$$

with L_{eff} (*effective length*) and $\bar{b}$ defined as $L_{eff} = L/w_C$ and $\bar{b} = b/ w_C$. Moreover, Christopher et al. demonstrated as the capillary number Ca plays a key role in determining the geometrical sizes of droplets generated in a T-shaped circuit, since it strongly affects both the parameter $\bar{b}$ and the volume V of the droplet, accordingly to the relations

$$(1 - \bar{b})^3 = \bar{b} \cdot C_a \tag{3}$$

$$V_{eff} = \frac{\phi}{\beta} \cdot Ca^{1-\alpha} \tag{4}$$

where $V_{eff} = V/ (h \cdot w_c^2)$ is an effective volume and α and β are constant factors. That being so, the performances of the microfluidic circuit can be verified by checking the dependence of L_{eff} and V_{eff} with respect to the flux ratio ϕ and the capillary number C_a, respectively.

The droplet length L was estimated by analysing each droplet image extracted from a video (minimum number of analysed droplet equal to 200). The value of L was determined referring to the front and back menisci of each droplet and further details of the data analysis procedure can be found in [14], where it was also demonstrated that in our T-junction the dispersion of L, obtained as the standard deviation of the length distribution, is of order of 1-3%. The results obtained are reported in Fig.1, where for each value of Q_C the flux of the dispersed phase Q_D was properly set in order to investigate values of flux ratio ranging between 0.1 and 2. Moreover, the dependence of L_{eff} with respect to ϕ was investigated for a surfactant concentration in the continuous phase equal to 0 (Fig.3-a) and 0.08% w/w (Fig.3-b).

The predictions of Eq.2 are well verified both with and without the SPAN®80 in the continuous liquid phase, even if Fig. 3b (i.e. in presence of the surfactant) shows some deviations at lower values of Ca, where anyway the theory of Christopher was not truly representative[17]. However, the low length droplets dispersion and the verification of the validity of Eq.2 suggest that $LiNbO_3$-based T-junction droplet generator stage has good and reproducible performances, better than those reported in PDMS-based microfluidic devices, especially if one considers that high droplet frequency generation can be achieved surely up to 1157±9 Hz, as already reported in [14].

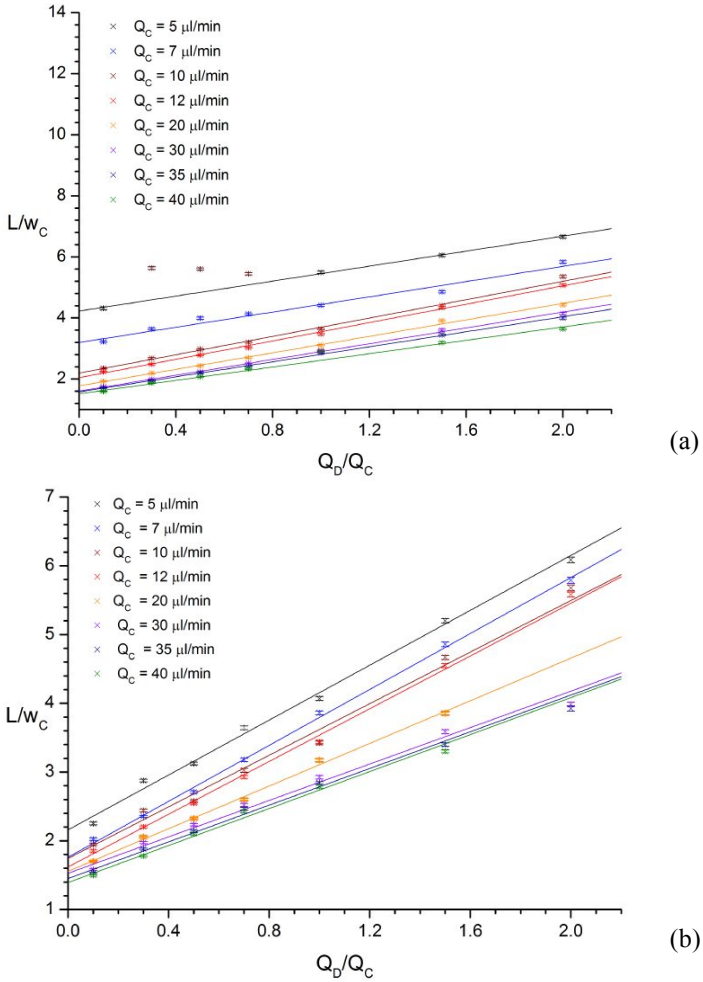

Fig.3 Dependence of L/w_C in absence of surfactant (a) and with surfactant concentration equal 0.08% (w/w) (b) as function of flux Q_C of the continuous phase (hexadecane).

Moreover it is possible to observe that the slope $\Lambda/\bar{b}$ of the linear fit is larger if the surfactant is added to the hexadecane, which can be explained by supposing a decrease of the value of geometrical parameter $\bar{b}$ with respect to the experiments performed without surfactant. As a matter of fact, since the presence of the SPAN®80 results in a reduction of the surface energy σ between the two liquids, a increasing of the capillary number C_a is expected, which in turn results in a lower value of $\bar{b}$, as predicted by Eq.1 and Eq.3.

Besides the length of the droplets, also the control over the volume is a critical parameter for many microfluidic applications, like chemical micro-reactors or biological photoluminescence sensors. Therefore, in this work also the relation between the volume of the droplet V and the capillary number C_a of the microfluidic system was investigated. The volume V can be estimated by fitting the droplet shape, taking into account that the menisci zone is well described by and ellipsoid, so that the following equation holds

$$V_{droplet} = L \cdot h \cdot w_C - 2\left[\frac{w_C{}^2 h}{2} - \frac{2}{3}\pi\frac{w_C{}^2 h}{8}\right] \quad (5)$$

and consequently the effective volume V_{eff} can be related directly to L_{eff} by

$$V_{eff} = \frac{V_{droplet}}{w_C{}^2 h} = L_{eff} - \frac{6-\pi}{6} \quad (6)$$

In Fig.4 the dependence of V_{eff} on the capillary number C_a is reported, both in presence and in absence of surfactant in the continuous phase. For both the set of data the values of the volume V are of the order of nanoliters, ranging from 1.7 nL to 5.9 nL. It is possible to observe that the two graphs present two different range of values of C_a: this is due to the presence of the surfactant that, as explained above, induces a reduction of the surface energy between the liquids, thus leading to a 5-times higher values of the capillary number if SPAN®80 is added to hexadecane (range between 0.002 and 0.016).
The results obtained show once more as the performance of our $LiNbO_3$-based T-junction confirm the Christopher's model, being the experimental results well fitted by Eq.4. In particular, it has to be mentioned that the first two points of Fig.4 (a) (red symbols) were not included in the fit, since the corresponding values of C_a lie out of the range of validity of the Christopher's model, that is for capillary number higher than $8 \cdot 10^{-3}$. Finally, the value of the parameter α derived by the fitting the experimental data in Fig.4 (a) can be compared with the corresponding value reported in [17], since the two values were both obtained in absence of surfactant. In our case $\alpha = (1.29 \pm 0.01)$, which is in good agreement with the value $\alpha_c = (1.31 \pm 0.03)$ obtained by Christopher and co-workers.

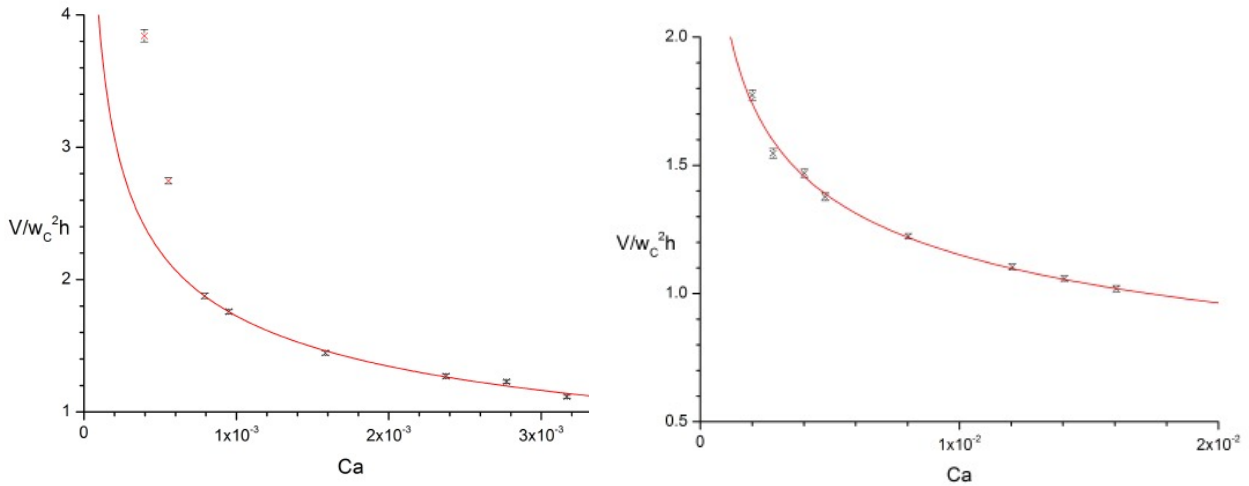

(a) (b)

Fig.4 Dependence of V_{eff} on the capillary number C_a both in absence of surfactant (a) and with a surfactant concentration of 0.08% w/w (b) added to the hexadecane.

3.1 Optical stage: waveguides characterization

The refractive index profile of an optical channel waveguide can be determined by means of different numerical approximations, such as the method of finite differences or finite elements, which can be used to calculate the effective refractive indices of the various modes guided by an assumed refractive index profile. Among others, also the method proposed by Strake et al. [19] allows to directly derive the refractive index profile of a Ti-diffused waveguide realized on a lithium niobate crystal by knowing the dopant concentration profile inside the substrate.
To properly tune the Ti concentration profile of the final waveguides, as first step several x-cut Ti-diffused $LiNbO_3$ samples were realized, by varying both the time of the Ti thin film deposition and that of the thermal treatments. In this way it was possible to derive the Ti diffusion coefficient at 1030°C, which is equal to $D_{Ti} = (88 \pm 8)$ nm^2/s, by means of Secondary Ion Mass Spectrometry measurements. The final in-depth Ti concentration profile is shown in Fig.5, where it is possible to observe as the whole doped layer is confined in few micrometers below the surface of the crystal, presenting a semi-gaussian profile as expected by Fick-type diffusion equation. The mean depth of the doped area and the dopant concentration at the surface of the $LiNbO_3$ substrate are $w = (1.13 \pm 0.05)$ μm and $C_s =$ 5% mol, respectively. Therefore, by using Strake's formula we derived a maximum refractive index change at the surface of the doped area which is equal to $\Delta n_e = (1.12 \pm 0.03) \times 10^{-2}$ and $\Delta n_o = (0.66 \pm 0.02) \times 10^{-2}$ for the

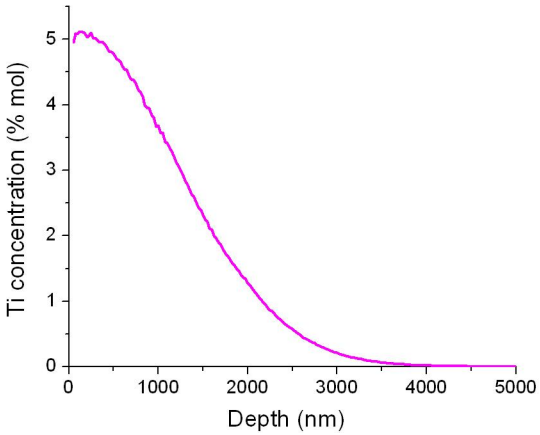

Fig.5: Ti in-depth profile of a planar waveguide realized in a lithium niobate substrate by thermally diffusing a Ti thin film. The profile was derived by using the SIMS technique.

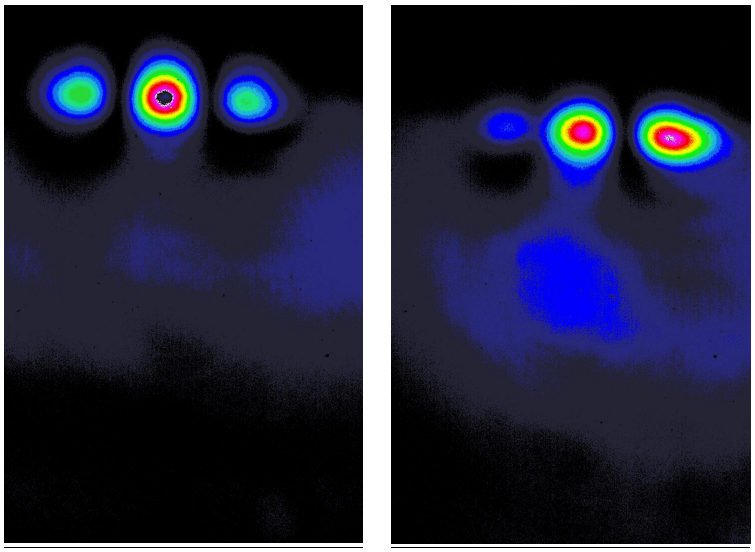

Fig.6 TE modes guided in a channel waveguide realized at the surface of a lithium niobate crystal by Ti in-diffusion. The channel width is equal to (9.8 ± 0.5) μm.

extraordinary and ordinary optical axis of the material, respectively.

Near-field measurements were carried out by connecting the digital camera to the computer and by controlling the intensity of the exiting beam after the fiber by using a diode laser driver. An objective 20x was exploited to couple the beam with the waveguide: at the entrance of the waveguide the waist of the beam was measured to be (5,30372 ± 1,1124) μm, with a maximum intensity of 2.2 x 10^5 W/m^2. A linear polarizer was positioned in front of the objective in order to selectively excite TE or TM modes.

Firstly, the channel waveguides with a width of about 10 μm were investigated. As expected from numerical simulations performed by the commercial software COMSOL Multiphysics®, these optical waveguides support multiple propagating modes at 670 nm, as it is shown in Fig.6, where the light intensity distribution of the TE mode exiting the waveguide is shown. As it is possible to observe, the guided modes present a well-defined shape, which is asymmetric in the vertical direction due to the fact that the Ti concentration in the doped area varies with depth, thus creating a gradient of the refractive index change along the diffusion direction. However, an unwanted surface guiding layer superimposes onto the Ti-diffused area and in principle this could significantly affect the performances of the final opto-fluidic device. As a matter of fact these waveguides were realized by performing the thermal

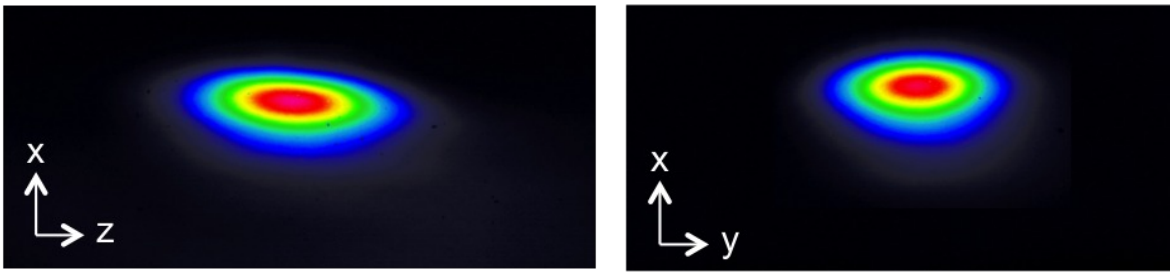

Fig.7 TE modes guided in channel waveguides realized at the surface of a lithium niobate crystal by Ti in-diffusion. The channel width is equal to (5.9 ± 0.2) μm and the propagation direction is along the y-axis (left) and the z-axis (right) of lithium niobate.

diffusion of the Ti stripes in air atmosphere, which could lead to a LiO_2 out-diffusion at the surface of the crystal, thus giving rise to a refractive index change with a gradual in-depth decrease approaching the bulk refractive index [20]. This problem can be solved by performing the diffusion treatments in O_2 atmosphere, thus preventing both the precipitation of $LiNbO_3$ into lithium triniobate ($LiNb_3O_8$) and the corresponding out-diffusion of LiO_2[21]. Therefore, new channel waveguides were prepared by realizing Ti strip with a width of (5.9 ± 0.2) μm and by thermally diffusing them in a dry oxygen atmosphere, in order to support a single-mode guided beam without the presence of a surface guiding layer. The final light intensity distribution is presented in Fig.7 for a TE guided beam propagating along the y-axis (left) and z-axis (right) of the substrate. As expected, both the channel waveguides support a single guided mode at 670 nm and the guiding layer at the surface of the crystal is not more present. Besides the vertical asymmetry of the light intensity distribution due to the semi-gaussian refractive index profile, as discussed above, the size of the two beams slightly differ in the transversal direction. This is due to the different crystallographic orientation of the two samples, as depicted in Fig.7. As a matter of fact, the Ti diffusion coefficient along y-axis of lithium niobate is about 1.5 times smaller than in the z-axis, as reported in [22], so that the final doped area has a larger transversal size in the y-propagating waveguides (Fig.6-left).

The final step to realize the optofludic device presented in this work is the integration on the same substrate of the T-junction with the optical waveguides. As a matter of fact, this goal was already achieved in the case of straight microfluidic channels realized in $LiNbO_3$ by means of optical grade dicing, as reported by the authors in [23], where a transmittance up to 0.5 is obtained when the channel is filled with hexadecane (n=1.43). However, the capability to integrate the optical waveguides also in microfluidic devices engraved by using the laser ablation method would pave the way for using lithium niobate also in other various opto-fluidic applications, where fluidic circuits with arbitrary shapes are required. Actually, a first attempt was already done, but both the shape of the beam as well as its transmitted light intensity after crossing the microfluidic channel (below 5%) are not satisfactory. In principle this could be partially attributed to the higher sidewall roughness of the channels engraved by laser ablation (R_a = (50.1 ± 3.2) nm) with respect to those realized by optical grade dicing (R_a = (6.8 ± 1.1) nm). Despite of this, both the values of R_a are lower than those typical of optofluidic devices realized in fused silica [24] and closed to those reported in[13], so this should not be a critical parameter in our case. Rather, it is more probable that the low coupling efficiency between the microfluidic channel and the optical waveguide is due to the fact that the optical stage was realized after the micromachining by laser ablation, thus making difficult the realization of well sharp Ti stripes at the edge of the fluidic channel walls, which results in a distorted and scattered beam when crossing the fluidic channel. Currently, new samples are being prepared in order to optimize the sidewall roughness of the microfluidic device.

4. CONCLUSIONS

Micro-fluidic channels were realized for the first time in x-cut lithium niobate crystals by means of laser ablation technique. A femtosecond laser operating at 800 nm, with a scanning velocity of 500 μm/s and a laser pulse energy of 5 μJ was exploited to create a T-shaped droplet generator, then sealed by a PDMS layer. The microfluidic

performance of this device was characterized in a wide range of droplet generation frequency, by investigating also the role played by the surfactant SPAN® 80 which can be added to the continuous liquid phase. Particular attention was paid on the reproducibility of droplet formation process, by studying the dependence of both their length and volume as a function of flux ratio and capillary number, respectively, and by comparing the obtained results with those expected by the theoretical model used for PDMS-based circuits. The results show that laser ablation is a suitable technique to get high performant microfluidic droplet generators completely engraved in lithium niobate substrates. Moreover, the Ti in-diffusion process combined with suitable photolitoghaphic patterning was used to realize channel waveguides in x-cut lithium niobate. Accordingly to the different width of the Ti-doped stripes, it was possible to create multiple-modes or single mode waveguides at 670 nm, whose light intensity distribution was characterized by means of near-field method. The good performances of both the microfluidic and the optical stages demonstrated the feasibility of an opto-fluidics device created on a single lithium niobate substrate to monitor the optical properties of droplet, thus paving the way for the use of this material in bio-sensing and chemical applications.

ACKNOWLEDGMENTS

The authors kindly acknowledge the Ca.Ri.Pa.Ro foundation for financing the research by the Excellence Project "Integrated opto-microfluidic prototype on lithium niobate crystals for sensing applications" (call 2011-2012) and the COST action MP1205 "Advances in Optofluidics: Integration of Optical Control and Photonics with Microfluidics".

REFERENCES

[1] McMullen J.P. and Jensen K.F., "Integrated microreactors for reaction automation: New approaches to reaction development", Annu. Rev. Anal. Chem. 3, 19-42 (2010);
[2] Watts P. and Haswell S.J., "The application of micro reactors for organic synthesis", Chem. Soc. Rev. 34, 235-246 (2005);
[3] Doku G. N., Verboom W., Reinhoudt D.N. and Van den Berg A., "On-microchip multiphase chemistry—a review of microreactor design principles and reagent contacting modes", Tetrahedron 61, 2733-2742 (2005);
[4] Psaltis D., Quake S. R. and Yang C., "Developing optofluidic technology through the fusion of microfluidics and optics", Nature 442, (2006);
[5] M. Sin, J. Gao, J. Liao and P. Wong, "System integration – A major step toward lab on a chip.", Jour. Biol. Eng. vol.5 p.1-21 (2011);
[6] Friend J.R. and Yeo L.Y., "Microscale Acoustofluidics: Microfluidics Driven via Acoustics and Ultrasonics", Rev. of modern Physics 83, 647-704 (2011);
[7] Tan M. K., Yeo L. Y. and Friend J. R., "Rapid fluid flow and mixing induced in microchannels using surface acoustic waves", EPL 87, 47003 (2009);
[8] Grilli S. and Ferraro P., "Dielectrophoretic trapping of suspended particles by selective pyroelectric effect in lithium niobate crystals", Appl. Phys. Lett. 92, 232902 (2008);
[9] Esseling M., Holtmann F., Woerdermann M. and Denz C., "Two-dimensional dielectrophoretic particle trapping in a hybrid crystal/PDMS-system, "Optics Express 18 (16), 17404 (2010);
[10] M. Jubera, A. García-Cabañes, J. Olivares, A. Alcazar and M. Carrascosa, "Particle trapping and structuring on the surface of LiNbO3:Fe optical waveguides using photovoltaic fields", Optics Letters 39, 649-652 (2014)
[11] Esseling, M., Zaltron, A., Sada, C., Denz, C. "Charge sensor and particle trap based on z-cut lithium niobate", Appl. Phys. Lett. 103, 061115-1-3 (2013)
[12] M. Esseling, A. Zaltron, W. Horn and C. Denz, "Optofluidic droplet router", Laser and Photonics Reviews 9 (1), 98-104 (2015)
[13] Sridhar, M., Maurya, D.K., Friend, J.R., Yeo, L.Y., "Focused ion beam milling of microchannels in lithium niobate", Biomicrofluidics 6 (1), 12819-128911 (2012)

[14] Pozza, G., Kroesen, S. , Bettella, G., Zaltron, A., Esseling, M., Mistura, G., Sartori, P., Chiarello, E., Pierno, M., Denz, C., Sada, C., "T-junction droplet generator realised in lithium niobate crystals by laser ablation", Optofluid. Microfluid. Nanofluid. 1, 34-42 (2014)
[15] E. Piccin, D. Ferraro, P. Sartori, E. Chiarello, M. Pierno and G. Mistura, "Generation of water-in-oil and oil-in-water microdroplets in polyester-toner microfluidic devices", Sensors and Actuators B 196, 525 (2014)
[16] Hu H., Ricken R. and Sohler W., "Low-loss ridge waveguides on lithium niobate fabricated by local diffusion doping with titanium", Appl. Phys. B 98, 677–679, (2010),
[17] G. F. Christopher, N. N. Noharuddin, J. A. Taylor and S. L. Anna, "Experimental observations of the squeezing-to-dripping transition in T-shaped microfluidic junctions", Physical ReviewE 78, 2008, 036317-1
[18] C. N. Baroud, F. Gallaire, and R. Dangla, "Dynamics of microfluidic droplets.," Lab Chip 10 (16), 2032–45 (2010)
[19] Strake E., Bava G.P. and Motrosset I., "Guided modes of Ti.LiNbO3 channel waveguides: a novel quasi-analytical technique in comparison with the scalar finite-element method", J. Lightwave Tech. 6 (6), 1126 (1998);
[20] M.N. Armenise, "Fabrication techniques of lithium niobate waveguides", IEEE PROCEEDINGS 135 (2), 85-91 (1988)
[21] M.V. Ciampolillo, A. Zaltron, M. Bazzan , N. Argiolas , C. Sada, S. Mignoni and M.Fontana, "Iron doping of lithium niobate by thermal diffusion from thin film: study of the treatment effect", Appl Phys A 104, 453–460, (2011)
[22] F. Caccavale, P. Chakraborty, A. Quaranta, I. Mansour, G. Gianello, S. Bosco, R. Corsini and G, Mussi, "Secondary-ion-mass spectrometry and near-field studies of Ti:$LiNbO_3$ optical waveguides", J. Appl. Phys. 78 (9), 5345-5350 (1995)
[23] G. Bettella, G. Pozza, A. Zaltron, M.V Ciampolillo, N. Argiolas, C.Sada, M. Chauvet and B. Guichardaz, "Integrated opto-microfluidics platforms in lithium niobate crystals for sensing applications", Proceeding of SPIE Photonics West, Feb. 2015
[24] R. Osellame, H. J. W. M. Hoekstra, G. Cerullo and M Pollnau, "Femtosecond laser microstructuring: an enabling tool for optofluidic lab-on-chips", Laser Photonics Rev. 5 (3), 442–463 (2011)
[25] P. Sivarajah, C. A. Werley, B. K. Ofori-Okai, K. A. Nelson, "Chemically assisted femtosecond laser machining for applications in LiNbO3 and LiTaO3", Appl. Phys. A, 2013, 112
[26] J-W Lee, Y.-K. Cho, M.-W. Cho, G.-H. Kim and T.-J. Je, "Optical transmittance recovery of powder blasted micro fluidic channels on fused silica glass using MR polishing", Intern. J. Precision Eng. and Man. 13 (2012)